HiSST: 3rd International Conference on
High-Speed Vehicle Science Technology
14 -19 April 2024, Busan, Korea

Investigation on the Linear Stationary Crossflow Stability Characteristics of Hypersonic Boundary Layer with Expansion Corner

Peisen Lu[1], Youcheng Xi[2], Song Fu[3]

Abstract

The expansion corner is a typical kind of structure on swept wings of hypersonic vehicles, which has a great effect on crossflow instabilities. This work aims to investigate the actual effect of the expansion corner on linear instabilities in practical three-dimensional hypersonic flow regimes. Hypersonic swept flows over a designed wing model of real vehicles are studied. The flow is calculated at a free-stream Mach number of 6 with the adiabatic wall condition. The model consists of a blunt cone, after which comes an expansion corner along with a flat plate. The corresponding laminar flow computations with different swept angles have been carried out using in-house shock-fitting procedures in order to ensure the quality of the base flow. Linear stability theory (LST) has been incorporated in investigating the effects of expansion corner on stationary crossflow instabilities. The most unstable mode which dominates the instability behaviour is calculated at interested streamwise locations. Both growth rates curves and neutral curves are provided to indicate the stability characteristics in this regime.

Keywords: *Hypersonic, Stability, Crossflow*

Nomenclature

LST – Linear stability theory
LNS – Linearized Navier-Stokes
DNS – Direct numerical simulation
Ma – Mach number
Re – Reynolds number
T – Temperature
Pr – Prandtl number
α – streamwise wave number
β – spanwise wave number
γ – Specific heat ratio
Λ – Sweep angle

1. Introduction

1.1. Research background

In the realm of aerodynamic studies, the instability and transition phenomenon of the boundary layer holds a prominent position as a typical flow phenomenon on aircraft surfaces. This phenomenon can lead to a significant increase in skin friction and heat flux, making it closely related to the design of the vehicle's thermal protection system. However, due to the strong nonlinearity and sensitivity of the flow itself, the transition of hypersonic flows still presents numerous challenges [1].

The three-dimensional boundary layer on the actual vehicle surface is subject to various instability mechanisms that can trigger transition, such as attachment line instability, streamwise instability, centrifugal Görtler instability, and crossflow instability, with crossflow stability being particularly important. Unlike two-dimensional boundary layers, the typical feature of three-dimensional boundary layers is that inviscid instabilities may dominate over traditional viscous instabilities, such as Tollmien-Schlichting (T-S) waves, as the primary instability mechanism [2]. Within this context, Hall [3] pointed out that the significance of centrifugal Görtler instability diminishes substantially when the sweep angle

[1] *Tsinghua University, Peking, China, loopersen@163.com*
[2] *Tsinghua University, Peking, China, xiyc@mail.tsinghua.edu.cn*
[3] *Tsinghua University, Peking, China, fs-dem@tsinghua.edu.cn*

surpasses a certain threshold relative to the Reynolds number raised to the power of one-half ($Re^{-1/2}$). Consequently, the dominant instability mechanisms become either T-S instability or crossflow instability.

Crossflow, a secondary flow in the three-dimensional boundary layer, is induced by an imbalance between the pressure gradient perpendicular to the potential flow direction and the centripetal force. This secondary flow has a velocity profile with an inflection point, making it primarily governed by the inviscid instability mechanisms defined in traditional stability analysis. Typical models for studying crossflow include swept wings, corner flows, swirling disks, and blunted cones with an angle of attack.

The stability characteristics of the three-dimensional boundary layer are often investigated using modal analysis methods. Crossflow modes can be classified into two overarching categories: stationary waves characterized by zero frequency, and traveling waves characterized by specific frequencies [4]. The most unstable traveling wave mode typically has a frequency much lower than that of the T-S mode and the second Mack mode. Stationary wave disturbances are commonly attributed to wall roughness-induced excitations, whereas traveling wave disturbances primarily arise due to the turbulence intensity within the freestream flow. Deyhle [5] pointed out that, despite the generally higher growth rates predicted by linear stability theory for traveling wave modes, empirical evidence suggests that in instances of low turbulence intensity in the incoming flow, the transition is often instigated by stationary wave modes. Therefore, studying the stability characteristics of steady crossflow modes can help understand the physical factors influencing transition under actual flight conditions.

Although there have been studies on hypersonic crossflow stability for various geometries such as flat plates and blunt cones, research on crossflow stability for complex models remains limited and insufficient. This study aims to utilize a linear stability framework to analyze the impact of typical expansion corner structures on the growth rate of the steady crossflow mode in a three-dimensional boundary layer, which further provides a theoretical basis for the analysis of the transition mechanism influenced by expansion corners on hypersonic vehicles.

1.2. Problem statement

To approximate the real wing shape of a hypersonic aircraft, the study focuses on a specially designed swept wing model. This model comprises a blunt cone with half-angle of 6 degrees followed by an expansion corner and a flat plate. The calculations are conducted at a free-stream Mach number of 6, under adiabatic wall conditions. The sweep angle ranges from zero to 60 degrees, and the present discourse exclusively presents outcomes pertaining to the 60-degree sweep angle configuration. The incoming flow conditions for calculation are based on the actual flight scenario, using the standard atmospheric physical parameters at an altitude of 27km as the reference quantity. The detailed working conditions are shown in Table 1.

Table 1. Calculation parameters

Re	**T_∞**	**R_{head}**	**Pr**	γ
3.521×10^6	224K	2mm	0.72	1.4

2. Methodology

2.1. Baseflow calculation

Hypersonic stability analysis requires high-quality laminar baseflow calculation. To obtain a smooth and accurate fundamental flow field, this paper employs a high-order accurate shock-fitted finite difference method for the calculation of the swept baseflow.

Since this method uses moving shocks as the far-field boundary, the program adopts a dynamic grid method, and there exists the following transform relationship between the physical coordinates and the computational coordinates:

$$\begin{cases} \xi = \xi(x,y,t) \\ \eta = \eta(x,y,t) \\ \zeta = z \\ \tau = t \end{cases}, \quad J = \begin{vmatrix} x_\xi & x_\eta & 0 & x_\tau \\ y_\xi & y_\eta & 0 & y_\tau \\ 0 & 0 & 1 & 0 \\ 0 & 0 & 0 & 1 \end{vmatrix} \tag{1}$$

The control equation is the Navier-Stokes equation for compressible fluids, which is expressed as follows:

$$\frac{1}{J}\frac{\partial U}{\partial \tau}+\frac{\partial F_{inv}}{\partial \xi}+\frac{\partial G_{inv}}{\partial \eta}+\frac{\partial H_{inv}}{\partial \zeta}+U\frac{\partial}{\partial \tau}\left(\frac{1}{J}\right)= \frac{1}{\mathrm{Re}}\left[\frac{\partial F_{vis}}{\partial \xi}+\frac{\partial G_{vis}}{\partial \eta}+\frac{\partial H_{vis}}{\partial \zeta}\right] \tag{2}$$

The expressions for the conservative variables, viscous flux and inviscid flux are:

$$U=\begin{bmatrix}\rho\\ \rho u\\ \rho v\\ \rho w\\ \rho E\end{bmatrix}$$
$$F_{inv}=\frac{F\xi_x+G\xi_y+H\xi_z}{J}, F=\begin{bmatrix}\rho u\\ \rho u^2+p\\ \rho uv\\ \rho uw\\ (E+p)u\end{bmatrix} \tag{3}$$

Besides, the working fluid is air, satisfying the assumptions of the ideal gas. The viscosity is calculated by Sutherland's law.The baseflow is calculated using in-house shock-fitting DNS code [6]. The fifth-order upwind scheme (for inviscid flux) of Zhong [7] together with the sixth-order centre scheme (for viscous flux) is used to compute the flow field. Here, the Rankine-Hugoniot relation is satisfied at the shock boundary. A fourth-order Runge–Kutta method is applied for the time integration. By treating the shock wave as a sharp interface, high accuracy can be achieved in the whole flow field, which is an essential prerequisite for the stability analysis.

2.2. Linear stability theory

The LNS equations are derived from the NS equations by introducing small perturbations, subtracting the basic flow equations and ignoring the nonlinear terms. A frequently employed form is commonly written as

$$\Gamma\frac{\partial \Phi}{\partial t}+\mathbf{A}\frac{\partial \Phi}{\partial x}+\mathbf{B}\frac{\partial \Phi}{\partial y}+\mathbf{C}\frac{\partial \Phi}{\partial z}+\mathbf{D}\Phi=\mathbf{H}_{xx}\frac{\partial^2 \Phi}{\partial x^2}+\mathbf{H}_{xy}\frac{\partial^2 \Phi}{\partial x\partial y}+\mathbf{H}_{xz}\frac{\partial^2 \Phi}{\partial x\partial z}+\mathbf{H}_{yy}\frac{\partial^2 \Phi}{\partial y^2}+\mathbf{H}_{yz}\frac{\partial^2 \Phi}{\partial y\partial z}+\mathbf{H}_{zz}\frac{\partial^2 \Phi}{\partial z^2} \tag{4}$$

Under the parallel flow assumption, the perturbations can be expressed in wave form:

$$\Phi(x,y,z,t)=\phi(y)\exp(i\alpha x+i\beta z-i\omega t)+\text{c.c.} \tag{5}$$

As only stationary waves are investigated, ω is assumed to be zero. The generalized eigenvalue problem of LST presents

$$\mathcal{L}_1\phi=\alpha\mathcal{R}_1\phi \tag{6}$$

2.3. Grid generation algorithm

The computational grid is a curvilinear body-fitted structured code-generated grid. The meshing strategy ensures a smooth transition in the distribution of grid spacing in the flow direction, and the spacing is densified near the leading edge and the expansion corner. The streamwise grid spacing is determined by

$$F=\sum_{i=1}^{4}a_i\mathrm{erf}\left[\sigma_i\left(\xi-b_i\right)+(-1)^{e_i}\right]$$
$$x=x(\xi),\frac{d^2x}{d\xi^2}=\frac{F}{2\Delta_s}\frac{dx}{d\xi}, \tag{7}$$
$$x(0)=0,\ x(1)=1,\ \xi\in[0,1]$$

In the wall-normal direction, grids cluster near the wall surface in the following manner:

$$y=a\frac{1+\eta}{b-\eta},\ a=\frac{y_i y_{\max}}{y_{\max}-2y_i},\ b=1+\frac{2a}{y_{\max}},\ \eta\in[-1,1] \tag{8}$$

The distribution of the spacing in the streamwise direction and the overall glance of the grid is shown in Fig. 1. After testing the grid independence, the final grid number is 1001×201.

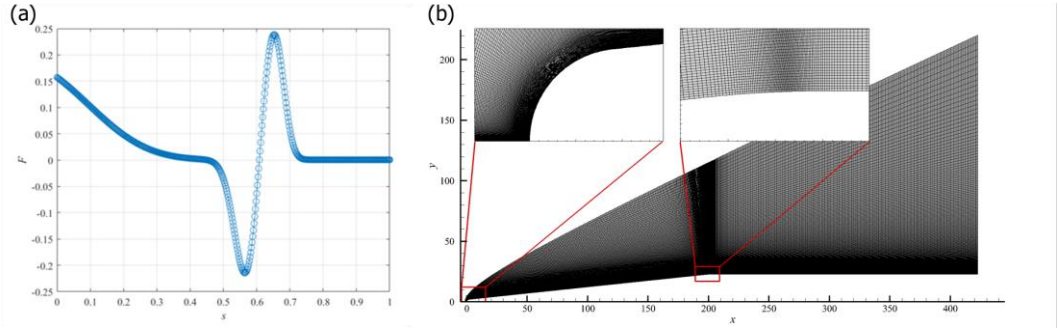

Fig 1. Computational grid of the swept wing model (a) the distribution of function F; (b) grid lines.

3. Results and discussion

3.1. Baseflow profiles

The results of our basic flow calculations are presented in Fig. 2. Our specialized shock-fitting DNS code ensures accurate depiction of the flow patterns. The expansion corner sharply increases the boundary layer thickness, and the effect of expansion waves are clearly seen.

Fig. 3 shows the velocity, density, and temperature profiles at typical locations before and after the expansion corner. It can be observed from the figure that the flow parameters conform to the predicted trend of the Prandtl-Meyer theory when passing through the expansion corner, and the change becomes smoother due to the viscous interference brought by the boundary layer. The streamwise velocity gradient parallel to the wall near the wall decreases first and then increases, overall resulting in an increase in velocity. The density decreases significantly overall, and the temperature decreases, with the boundary layer thickness monotonically increasing.

Fig. 4 provides the crossflow velocity U_{cf} profile at typical locations before and after the expansion corner, showing that the overall crossflow velocity decreases, but the crossflow velocity profile is fuller around s=101, with a stronger gradient in the near-wall region.

Fig. 5 presents the $D(\rho DU_{cf})$ distribution of the crossflow velocity profile before and after the expansion corner at typical locations, where D represents the differential with respect to the normal coordinate. According to the definition of the general inflection point, $D(\rho DW)=0$, from the curve in the figure, it can be seen that before the expansion corner at s about 90, there exist multiple general inflection points in the cross-flow profile. As the flow gradually approaches the expansion corner, the number of inflection points in the cross-flow profile gradually decreases, and at s about 111.8, only one general inflection point remains in the cross-flow profile. Further downstream, at s about 142, the flow recovers to three general inflection points.

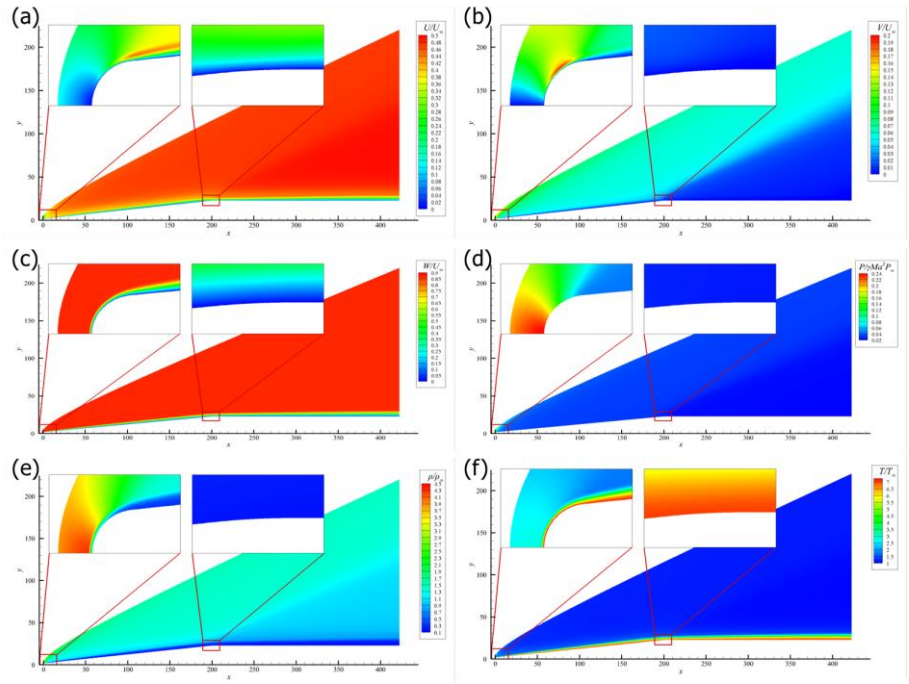

Fig 2. Contour of dimensionless parameters at Λ=60° (a) U velocity; (b) V velocity; (c) W velocity; (d) pressure; (e) density (f) temperature.

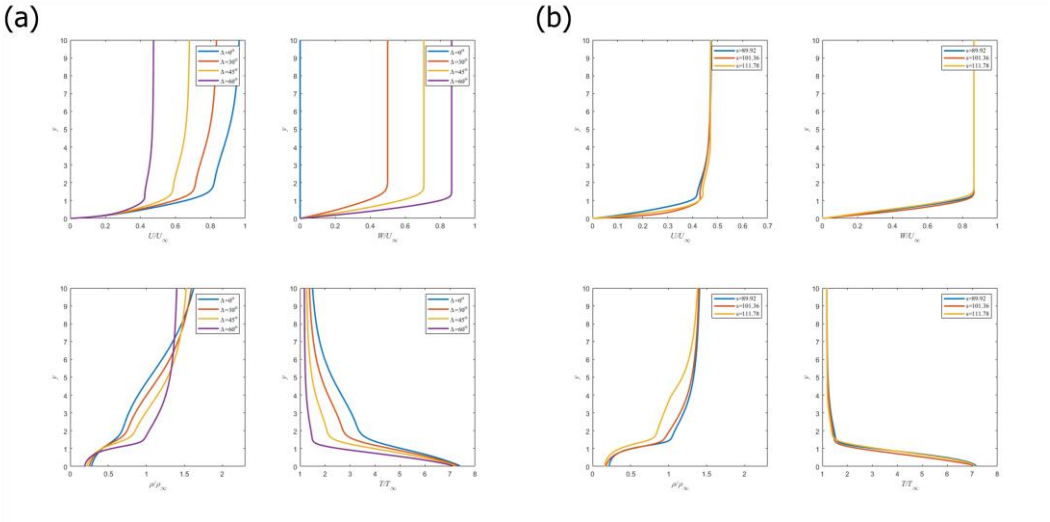

Fig 3. Profiles of physical parameters for (a) different sweep angles Λ at s=101.36; (b) different streamwise positions at Λ=60°.

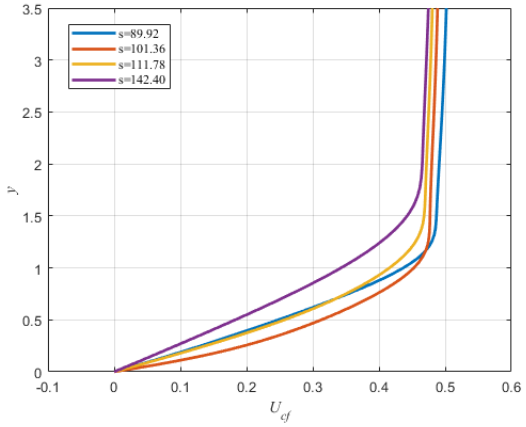

Fig 4. Profiles of crossflow velocity at different streamwise positions around the expansion corner

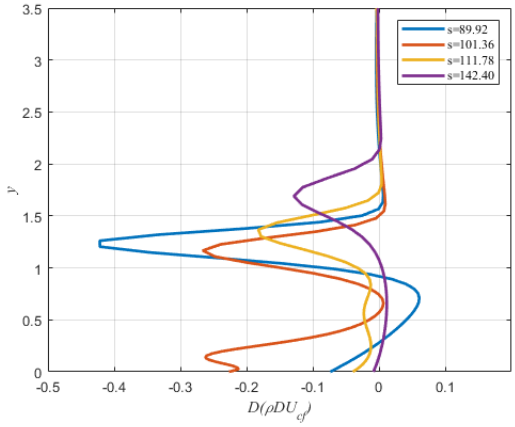

Fig 5. Profiles of $D(\rho DU_{cf})$ at different streamwise positions

3.2. Stability characteristics

The most unstable mode embodies the typical crossflow mode pattern. Fig. 4 shows the pattern of the most unstable perturbation mode at s=89.92, β=0.797. Fig. 4(a) provides the spectrum of the stationary wave. The spectrum consists of both discrete modes and continuous spectrum approximated by discrete points. Under this paper's working condition, there is only one unstable mode in the eigenvalue spectrum. As can be seen from the distribution of its eigenfunctions, the disturbance velocity components in the streamwise direction alternate in opposite peaks along the spanwise direction. Superimposed on the basic flow, this results in a series of streamwise vortical structures, which are characteristic of steady crossflow modes.

After the expansion corner, the crossflow vortices undergo a discernible transformation, assuming a more pronounced inclination and concurrently exhibiting an escalated growth rate, as is shown in Fig. 7. The figure presents the comparison of growth rate versus varying spanwise wave numbers at different streamwise positions. As the baseflow advances downstream, the spanwise wave number of the most unstable disturbance wave gradually decreases. The growth rate of the most unstable disturbance mode first decreases gradually with the advancement of the streamwise position and then starts to increase slowly as the basic flow passes through the expansion corner, which may possibly promote transition under this circumstance.

To further investigate the stability characteristics of the flow field, Fig. 8 provides the linear stability neutral curve. The abscissa represents the streamwise Reynolds number, and the ordinate represents the spanwise wave number. The yellow area represents the stable region where there are no unstable disturbance modes. When the streamwise Reynolds number is approximately 4.3×10^5, the flow passes through the expansion corner, and a new peak in the growth rate can be observed at this location. This indicates that as the flow advances through the expansion wave, the disturbances within the boundary layer become more unstable.

Further analysis and comparison are conducted on the specific characteristics of the most unstable disturbance waves before and after the expansion corner. Fig. 9 presents the shape functions and streamwise velocity contours of the most unstable stationary modes at two typical streamwise positions. These two modes come from the areas near the two peaks of the growth rates shown in Fig. 8. Observing the disturbance velocity contour maps of both in Fig. 9(b), it can be noticed that their main features are similar, exhibiting the typical characteristics of the crossflow mode. However, from the specific disturbance velocity characteristic functions in Fig. 9(a), significant differences can be found between them in terms of sign changes.

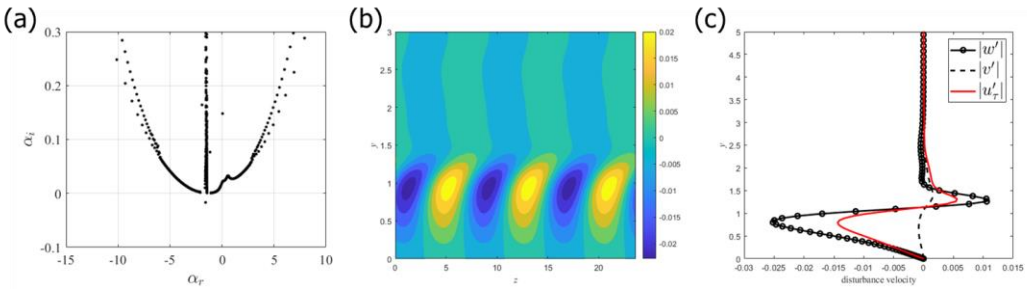

Fig 6. The most unstable mode at *s*=89.92 (a) eigenvalue spectrum; (b) contour of streamwise velocity; (c) shape function of perturbation velocity.

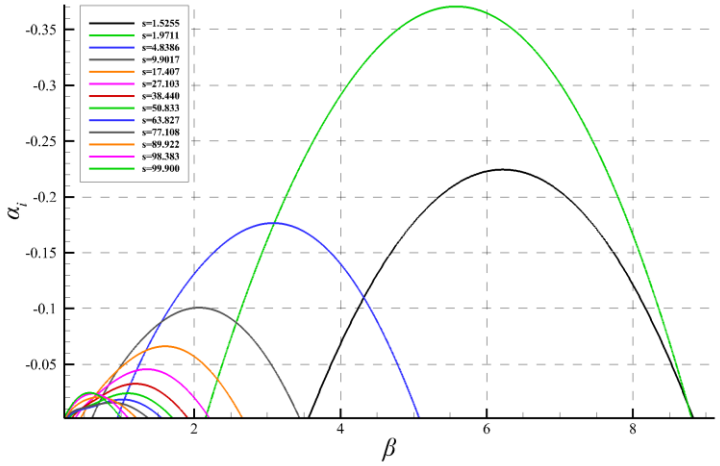

Fig 7. Growth rate curves at different positions with respect to the spanwise wavenumber β

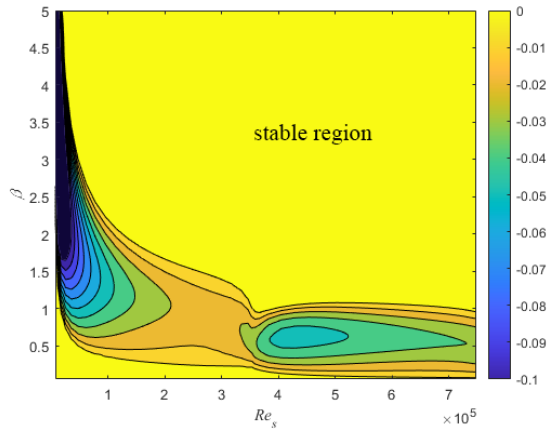

Fig 8. Neutral curve of the stationary perturbation modes

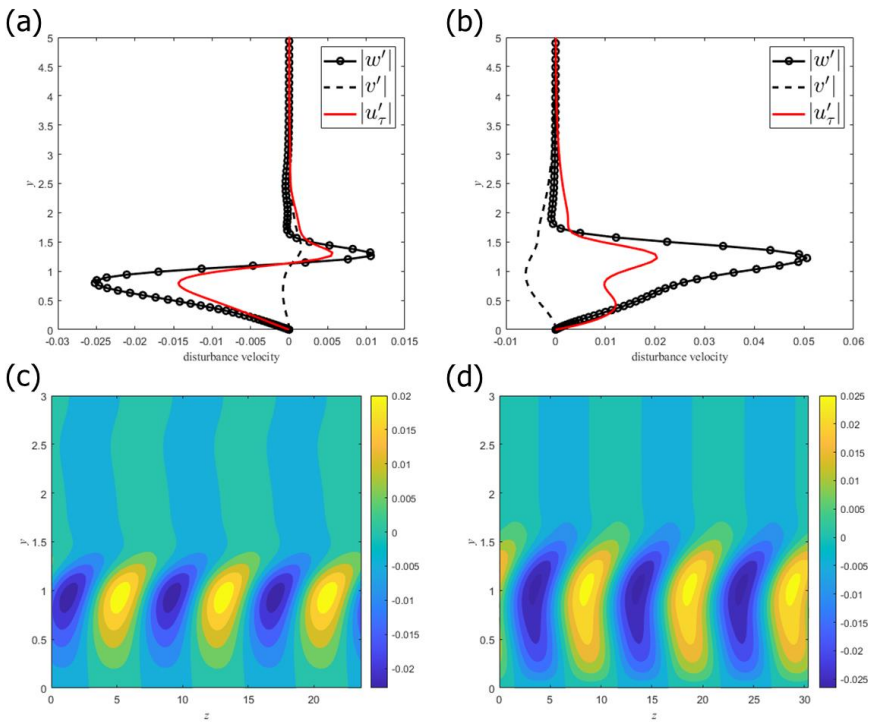

Fig 9. Comparison of the stationary perturbation modes (a-b) perturbation velocity at s=89.92,121.79; (c-d) streamwise velocity contour at s=89.92,121.79.

Theoretical and experimental studies generally suggest that expansion waves can stabilize flows. Chuvakhov [8] conducted a linear stability analysis of two-dimensional expansion corners and found that in the absence of sweep angle, the second mode dominates. The main effect of the expansion corner on stability characteristics is the increase in boundary layer thickness, which significantly reduced the frequency of the second mode disturbance waves. The growth rates of the high-frequency modes decreased sharply across the corner, while the previously stable low-frequency modes became unstable, leading to a more stable flow phenomenon. In contrast, this study on stationary crossflow modes reaches opposite conclusions. According to Fig. 10, on the wedge surface after the blunt head, as the flow progressed in the streamwise direction, the growth rates of the unstable crossflow modes gradually decreased, and the number of general inflection points of the crossflow profile before the expansion wave decreased from three to one. As the flow passed through the expansion wave, the expansion wave caused significant changes in the distribution of flow parameters such as density and temperature, and the number of general inflection points of the crossflow recovered. This stimulation of specific boundary layer steady crossflow modes led to increased instability of the basic flow. In the downstream flat plate stage after the expansion corner, as the boundary layer continued to develop downstream, the growth rate of disturbances decreased again.

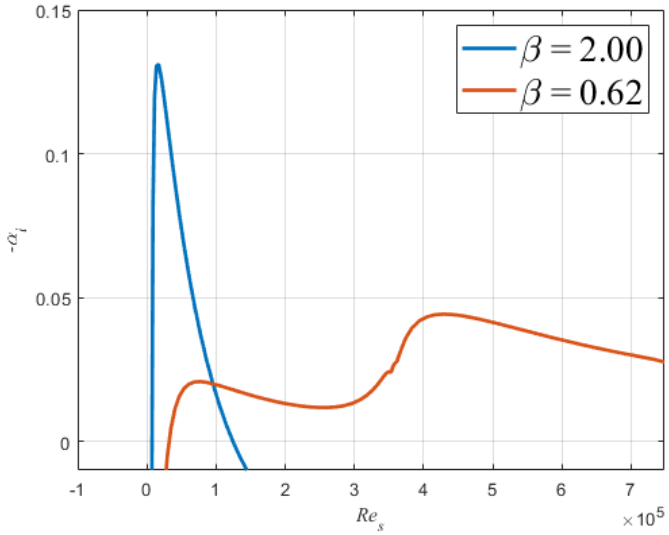

Fig 10. Growth rate versus streamwise Reynolds number for different spanwise numbers

4. Conclusion

This work preliminarily investigates the effect of expansion corner on the linear stability of the swept wing hypersonic boundary-layer flow. The high-accuracy baseflow of a swept wing with an expansion corner is calculated using the finite difference shock-fitting method. Based on this, linear stability tools are employed to explore the influence of the expansion corner on the linear instability characteristics of the stationary crossflow modes in the hypersonic boundary layer.

The shock-fitting method provides accurate and smooth baseflow. At the expansion corner, there is a significant change in the number of general inflection points in the streamwise velocity profile, which affects the inviscid instability characteristics of the boundary layer.

Under the working condition of this paper, the most unstable disturbance mode in the swept wing boundary layer before and after the expansion corner is the stationary crossflow mode. There is a significant change in the disturbance velocity characteristics of the stationary crossflow mode before and after the expansion corner.

The stationary crossflow mode before the expansion corner gradually decays in growth rate as it develops in the streamwise direction. The appearance of the expansion wave makes the stationary crossflow mode more unstable, and after passing through the expansion corner, the flow stabilizes again as it develops in the streamwise direction. The result indicates that the existence of the expansion corner may greatly destabilize the laminar base flow and thus promote transition.

In the future, we will continue investigating the non-linear behaviour of unstable modes which have been identified in this study. We plan to employ secondary instability theory (SIT) to monitor the change of secondary modes in the neighbourhood of the expansion corner. Furthermore, we would conduct a DNS study to compare the results with SIT.

5. Acknowlegements

Support from the National Key Research and Development Plan of China through project No. 2019YFA0405200, the National Key Project (Grant No. GJXM92579), NSFC grant 12202242 and 12172195, Yancheng MetaStone Co. is gratefully acknowledged.

References

1. Mack, L. M. Boundary-layer linear stability theory. Agard rep, 709(3), 1-3 (1984).

2. Reed, H. L., & Saric, W. S. Stability of three-dimensional boundary layers. Annual Review of Fluid Mechanics, 21(1), 235–284 (1989).
3. Hall, P.: The Görtler vortex instability mechanism in three-dimensional boundary layers. Proceedings of the Royal Society of London. A. Mathematical and Physical Sciences, 399(1816), 135-152 (1985).
4. Craig, S. A., Saric, W. S.: Crossflow instability in a hypersonic boundary layer. Journal of Fluid Mechanics, 808, 224-244 (2016).
5. Deyhle, H., Bippes, H.: Disturbance growth in an unstable three-dimensional boundary layer and its dependence on environmental conditions. Journal of Fluid Mechanics, 316, 73-113 (1996).
6. Xi, Y., Ren, J., Fu, S.: Hypersonic attachment-line instabilities with large sweep Mach numbers. Journal of Fluid Mechanics, 915, A44 (2021).
7. Zhong, X.: High-order finite-difference schemes for numerical simulation of hypersonic boundary-layer transition. Journal of Computational Physics, 144(2), 662-709 (1998).
8. Chuvakhov, P. V., Egorov, I. V., Ilyukhin, I. M., Obraz, A. O., Fedorov, A. V., & Fedorov, A. V. Boundary-layer instabilities in supersonic expansion corner flows. AIAA Journal, 59(9), 3398-3405 (2021).